
ELSEVIER
Volume 4 | Issue 8 | November 2011 | ISSN 1751-6161
Journal of the
Mechanical Behavior of
Biomedical Materials
Editor-in-Chief: David Taylor

JOURNAL OF THE MECHANICAL BEHAVIOR OF BIOMEDICAL MATERIALS 4 (2011) 1582–1594

Available online at www.sciencedirect.com

SciVerse ScienceDirect

journal homepage: www.elsevier.com/locate/jmbbm

Research paper

Modeling failure of soft anisotropic materials with application to arteries

K.Y. Volokh

Faculty of Civil and Environmental Engineering, Technion – Israel Institute of Technology, Haifa 32000, Israel

ARTICLE INFO

Article history:
Published online 26 January 2011

Keywords:
Fiber-reinforced composite
Anisotropy
Soft matter
Artery
Failure
Energy limiters

ABSTRACT

The arterial wall is a composite where the preferred orientation of collagen fibers induces anisotropy. Though the hyperelastic theories of fiber-reinforced composites reached a high level of sophistication and showed a reasonable correspondence with the available experimental data they are short of the failure description. Following the tradition of strength of materials the failure criteria are usually separated from stress analysis. In the present work we incorporate a failure description in the hyperelastic models of soft anisotropic materials by introducing *energy limiters* in the strain energy functions. The limiters provide the saturation value for the strain energy which indicates the maximum energy that can be stored and dissipated by an infinitesimal material volume. By using some popular constitutive models enhanced with the energy limiters we analyze rupture of a sheet of arterial material under the plane stress state varying from the uniaxial to equal biaxial tension. We calculate the local failure criteria including the maximum principal stress, the maximum principal stretch, the von Mises stress, and the strain energy at the moment of the sheet rupture. We find that the local failure criterion in the form of the critical strain energy is the most robust among the considered ones. We also find that the tensile strength – the maximum principal stress – that is usually obtained in uniaxial tension tests might not be appropriate as a failure indicator in the cases of the developed biaxiality of the stress–strain state.

1. Introduction

The arterial wall is an anisotropic inhomogeneous structure undergoing large deformations. These features make the phenomenological modeling of the arterial wall a challenging task. Nonetheless, huge progress has been made in the constitutive theories of arteries and, in a wider perspective, of soft biological tissues: Fung (1993); Humphrey (2002); Cowin and Humphrey (2002); Holzapfel and Ogden (2003, 2006, 2010). Some issues, however, require further elaboration. Among them is a theoretical description of failure.

Two approaches to predict failure of soft materials and biological tissues are used in the literature. The first – the strength-of-materials approach – is based on a pointwise criticality condition. According to this approach, a structure is analyzed by using constitutive models that do not include a failure description – the intact material models – and failure is claimed when a local failure criterion is obeyed at a material point. There are various local criteria as, for example, the maximum von Mises stress; the maximum principal stress; the maximum strain energy etc. Evidently, the strength-of-materials approach is simple yet restrictive because the

E-mail address: cvolokh@technion.ac.il.

1751-6161/$ - see front matter © 2011 Elsevier Ltd. All rights reserved.
doi:10.1016/j.jmbbm.2011.01.002

local state of deformation defines global failure, which is not necessarily correct. Moreover, the critical failure criteria are separated from stress analysis and their experimental validation is difficult.

The second – Continuum Damage Mechanics (CDM) – approach allows modeling global failure and includes the failure condition in its constitutive description. In CDM a scalar or tensor damage parameter is introduced to describe the degradation of material properties during mechanical loading (Hokanson and Yazdami, 1997; Rodriguez et al., 2006; Calvo et al., 2006; Balzani et al., 2006). The damage parameter is an internal variable whose magnitude is constrained by the damage evolution equation and the critical threshold condition analogously to theories of plasticity. Theoretically, the approach of damage mechanics is very flexible. Practically, the experimental calibration of damage theories might be very complicated because the damage parameter is hard to observe explicitly.

Recently, an alternative to the mentioned approaches emerged, which is based on the hyperelastic constitutive equations including the energy limiters—the softening hyperelasticity (Volokh, 2007, 2008a). This new approach is simpler than CDM because it involves neither internal variables nor their critical threshold condition and evolution equations. At the same time, contrary to the strength-of-materials approach the elasticity with energy limiters is a constitutive theory incorporating a failure description in the strain energy function which allows modeling the global failure.

In the present work we use the elasticity with energy limiters for modeling failure of soft anisotropic materials with emphasis on arteries. We propose three generalizations of the well-known arterial models by enforcing the failure descriptions. The first one generalizes the celebrated Fung model of the arterial wall. Two others generalize the popular Holzapfel–Gasser–Ogden (HGO) model based on the presentation of the characteristic directions of anisotropy by structural tensors. The proposed models are used to analyze failure in tension of an arterial sheet under the varying biaxiality conditions. The analysis allows us to reassess the local strength-of-materials criteria of the arterial failure.

The paper starts with a short review of elasticity with energy limiters in Section 2. The generalized Fung model is considered in Section 3. Two versions of the generalized HGO model are considered in Sections 4 and 5 accordingly. The discussion of the applicability of the local failure criteria appears in Section 6.

2. Elasticity with energy limiters

Let us consider the interaction of two particles, which can be molecules or molecular clusters. The reference distance between them corresponds to zero interaction force and zero stored energy. The interaction passes three stages with the increase of the distance. At the first stage the force increases proportionally to the increasing distance: the linear stage. At the second stage the force–distance relationship deviates from the linear proportionality: the nonlinear stage. At the third stage the force drops with the increasing distance: the separation or failure stage. In the case of solids composed of many particles two first stages of the particle interaction are described by the linear and nonlinear theories of elasticity correspondingly where the changing distance between particles is averaged by a continuum strain measure and the energy of the particle interaction is averaged by a strain energy function. Amazingly, the third, failure, stage of the particle interaction is beyond the scope of the traditional elasticity theories.[1] However, the failure description can still be introduced in elasticity by analogy with the failure description in the particle interaction. Indeed, the force of the pair interaction decreases with the increase of the interaction distance because the energy that can be stored during separation is limited by the constant of the bond energy. If the energy limiter exists for the pair interaction then it should exist in the multiple interactions. The latter means that we should limit the magnitude of the strain energy in order to describe material failure within the framework of elasticity.[2]

A very simple way to introduce the energy limiters is by using the following formula for the strain energy (Volokh, 2007)

$$\psi(\Phi, W) = \Phi\left\{1 - \exp\left(-\frac{W}{\Phi}\right)\right\}, \tag{2.1}$$

where W is the strain energy of an intact, i.e. without failure, material and Φ is the volumetric failure energy—the energy limiter. Formula (2.1) has two limit cases. If the failure energy is infinite, $\Phi = \infty$, then we have the classical hyperelastic material: $\psi(\infty, W) = W$. If the failure energy is finite then the increase of the strain energy is limited: $\psi(\Phi, \infty) = \Phi$.

An example of the use of (2.1) can be found in Volokh and Vorp (2008) for the incompressible material of the Abdominal Aortic Aneurysm (AAA) with the intact strain energy in the form

$$W = \alpha_1(\lambda_1^2 + \lambda_2^2 + \lambda_3^2 - 3) + \alpha_2(\lambda_1^2 + \lambda_2^2 + \lambda_3^2 - 3)^2, \quad J = \lambda_1\lambda_2\lambda_3 = 1 \tag{2.2}$$

where λ_is are the principal stretches and material constants $\alpha_1 = 10.3$ N/cm^2; $\alpha_2 = 18.0$ N/cm^2; $\Phi = 40.2$ N/cm^2 were calibrated in the uniaxial tension test shown in Fig. 1.

It is evident from Fig. 1 that formula (2.1) is useful for a description of smooth failure[3] with a flat limit point on the stress–strain curve, which corresponds to a gradual process of the bond rupture. In the case of more abrupt bond ruptures, however, a much sharper transition to the material instability occurs. To describe such sharp transition to failure (2.1) can be generalized as follows (Volokh, 2010a)

$$\psi = \frac{\Phi}{m}\left\{\Gamma\left(\frac{1}{m}, 0\right) - \Gamma\left(\frac{1}{m}, \frac{W^m}{\Phi^m}\right)\right\}. \tag{2.3}$$

where the upper incomplete gamma function $\Gamma(s, x) = \int_x^\infty t^{s-1}\exp(-t)dt$ is used.

The new material parameter m controls the sharpness of the transition to material instability on the stress strain curve.

[1] Short reviews of nonlinear elasticity with examples can be found in Beatty (1987) and Ogden (2003), for instance.

[2] It should not be missed that significant plastic deformations are beyond the scope of elasticity with energy limiters.

[3] Other examples are reviewed in Volokh (2008a).

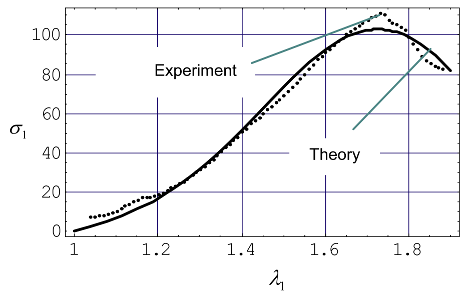

Fig. 1 – Cauchy stress [N/cm^2] versus stretch in the uniaxial tension of AAA material (from Volokh and Vorp, 2008).

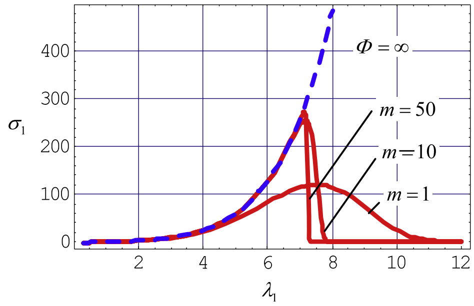

Fig. 2 – Cauchy stress [MPa] versus stretch in uniaxial tension of NR: blue dashed line designates the intact model; red lines designate the model with energy limiters for varying m.

Increasing m it is possible to simulate more brittle ruptures of the internal bonds. It should not be missed that (2.3) reduces to (2.1) for $m = 1$.

It is worth emphasizing again that by the sharp ($m > 10$) transition to material instability we mean the rupture of ideal bonds within a representative volume. Some materials have bonds that tear gradually and the stress–stretch curve goes down gently while other materials have bonds that tear abruptly and the stress–stretch curve goes down steeply. We do not consider localization into cracks which is a result of the imperfect material structure. It is clear, however, that such localization should happen near the limit point of the idealized stress–stretch curve.

Formula (2.3) was applied to a filled Natural Rubber (NR) vulcanizate with the following intact strain energy

$$W = \sum_{k=1}^{3} C_{k0}(\lambda_1^2 + \lambda_2^2 + \lambda_3^2 - 3)^k, \qquad J = \lambda_1\lambda_2\lambda_3 = 1, \tag{2.4}$$

where λ_i are principal stretches and $C_{10} = 0.298$ MPa, $C_{20} = 0.014$ MPa, $C_{30} = 0.00016$ MPa.

Based on the experiments by Hamdi et al. (2006), who found the critical failure stretch in uniaxial tension: $\lambda_c = 7.12$, the energy limiters $\Phi_1 = 74.4$ MPa, $\Phi_{10} = 82.0$ MPa, $\Phi_{50} = 69.63$ MPa were calibrated for varying parameter $m = 1, 10, 50$— Fig. 2.

The strain energy (2.3)–(2.4) calibrated in the uniaxial tension test was also examined under the biaxial tension and the results were compared to the biaxial tension tests conducted by Hamdi et al. (2006). The results of the comparison are presented in Fig. 3. It is not surprising that the critical experimental stretches presented in the center of Fig. 3 are slightly lower than the theoretical prediction because the equal biaxial stretching is very sensitive to imperfections in specimens and loads. The latter sensitivity is the reason why the equal biaxial failure tests are so difficult to perform. It seems like this situation is similar to the celebrated shell buckling problem which was a source of controversy for a long period unless it was realized that the critical buckling load was very sensitive to imperfections.

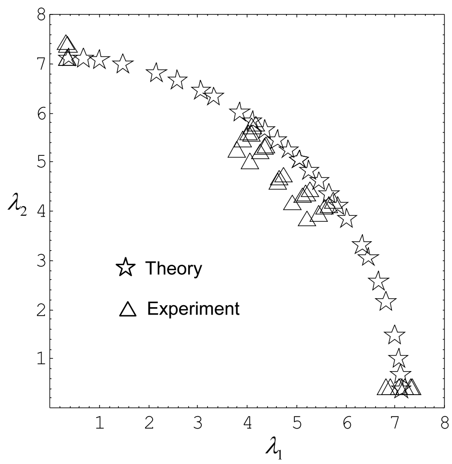

Fig. 3 – Critical failure stretches in biaxial tension for NR.

At this point we have to emphasize that the elasticity with energy limiters does not include a description of the energy dissipation in its theoretical setting. Such a description is irrelevant for the static problems considered in the present work because no unloading occurs. However, the account of the dissipation is crucial for modeling dynamic failure where the elastic unloading can potentially lead to the healing of the damaged material. Indeed, the unloading path should follow the same stress–strain curve as the loading path in the case of hyperelasticity and, consequently, no dissipation occurs and material heals. To prevent from the healing, the dissipation is easily enforced computationally by removing the failed finite elements from the mesh. Thus, the account of the dissipation is a technical rather than a theoretical issue—see Trapper and Volokh (2010) and Volokh (2011), for example.

Based on the presented AAA and NR models it is possible to calculate the critical rupture states of the material sheet, where $\partial^2\psi/\partial\lambda_1^2 \cdot \partial^2\psi/\partial\lambda_2^2 - (\partial^2\psi/\partial\lambda_1\partial\lambda_2)^2 = 0$, under the varying biaxiality parameter

$$n = \ln\lambda_2/\ln\lambda_1, \tag{2.5}$$

where λ_1 and λ_2 are the principal stretches in the plane of the sheet.

Uniaxial Tension (UT) corresponds to $n = -0.5$; Pure Shear (PS) corresponds to $n = 0.0$; and the equal Biaxial Tension (BT) corresponds to $n = 1.0$. Figs. 4 and 5 present the failure criteria for the critical states of the sheet instability calculated for the considered constitutive models incorporating the energy limiters for AAA and NR ($m = 10$) materials accordingly.

Von Mises stress presented in the figures is calculated as follows: $\sigma = \sqrt{3(\boldsymbol{\sigma} : \boldsymbol{\sigma} - (\mathrm{tr}\boldsymbol{\sigma})^2/3)/2}$, where $\boldsymbol{\sigma}$ is the Cauchy stress tensor.

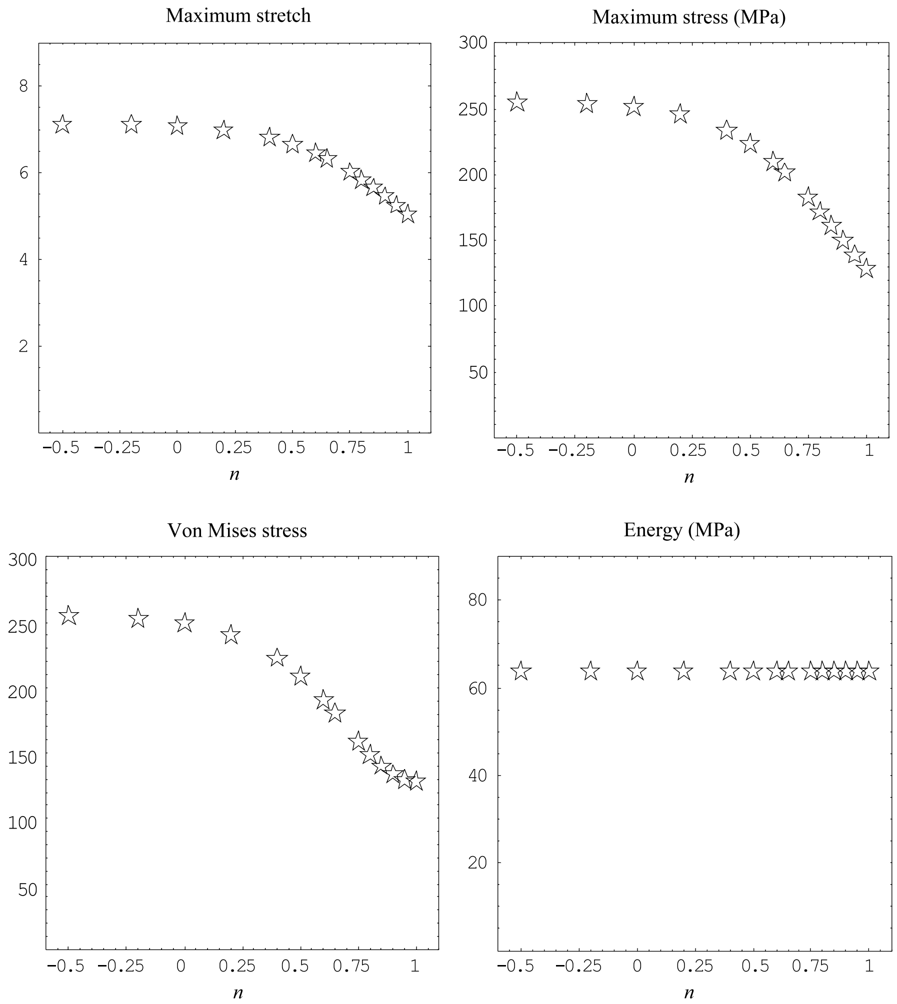

Fig. 4 – Critical failure criteria for Natural Rubber under varying biaxiality ratio.

Figs. 4 and 5 clearly show that only the energy criterion is almost constant for the critical failure states with varying biaxiality. It is especially crucial that critical parameters corresponding to uniaxial tension, which are usually fitted in experiments, decrease with the developing biaxiality. Thus, the rupture under equal biaxial tension occurs under smaller values of the critical parameters (except energy) than it is observed in uniaxial tension. This notion is very important because rubber-like materials and soft biological tissues are often loaded in the biaxial or triaxial stress–strain states in engineering and biological structures where the strength criteria based on uniaxial tension tests might not be applicable.

It should not be missed that all results concerning the reassessment of the local failure criteria presented in this section were obtained for isotropic materials. Arteries are anisotropic and we will examine the effect of anisotropy on their strength below. We also notice that AAA material is modeled as isotropic in Fig. 5 and in works by Volokh and Vorp (2008) and Volokh (2010b). However, the experimental analysis of Vande Geest et al. (2006) showed that the transition from the healthy artery to AAA can be accompanied by the increase of the material anisotropy. This conclusion is interesting and somewhat counterintuitive because we used to think that the formation of AAA is triggered by the degradation of the media layer which is the main source of anisotropy. Thus, one might probably expect the decrease of the arterial anisotropy with the development of AAA contrary to the data reported by Vande Geest et al. (2006). More light should be shed on this intriguing issue.

3. Enhanced Fung model

In a series of pioneering articles Fung developed the exponential strain energy functions W, which describe the intact deformation of the arterial wall (Fung et al., 1979; Chuong and Fung, 1983; Fung, 1993). Fung's model is incompressible and orthotropic and its generalized version incorporating failure can be written as follows

$$\psi = \frac{\Phi}{m}\left\{\Gamma\left(\frac{1}{m},0\right) - \Gamma\left(\frac{1}{m},\frac{W^m}{\Phi^m}\right)\right\}, \tag{3.1}$$

$$W = \frac{c}{2}(e^Q - 1), \tag{3.2}$$

$$Q = c_1E_{11}^2 + c_2E_{22}^2 + c_3E_{33}^2 + 2c_4E_{33}E_{22} + 2c_5E_{11}E_{22} + 2c_6E_{11}E_{33}, \tag{3.3}$$

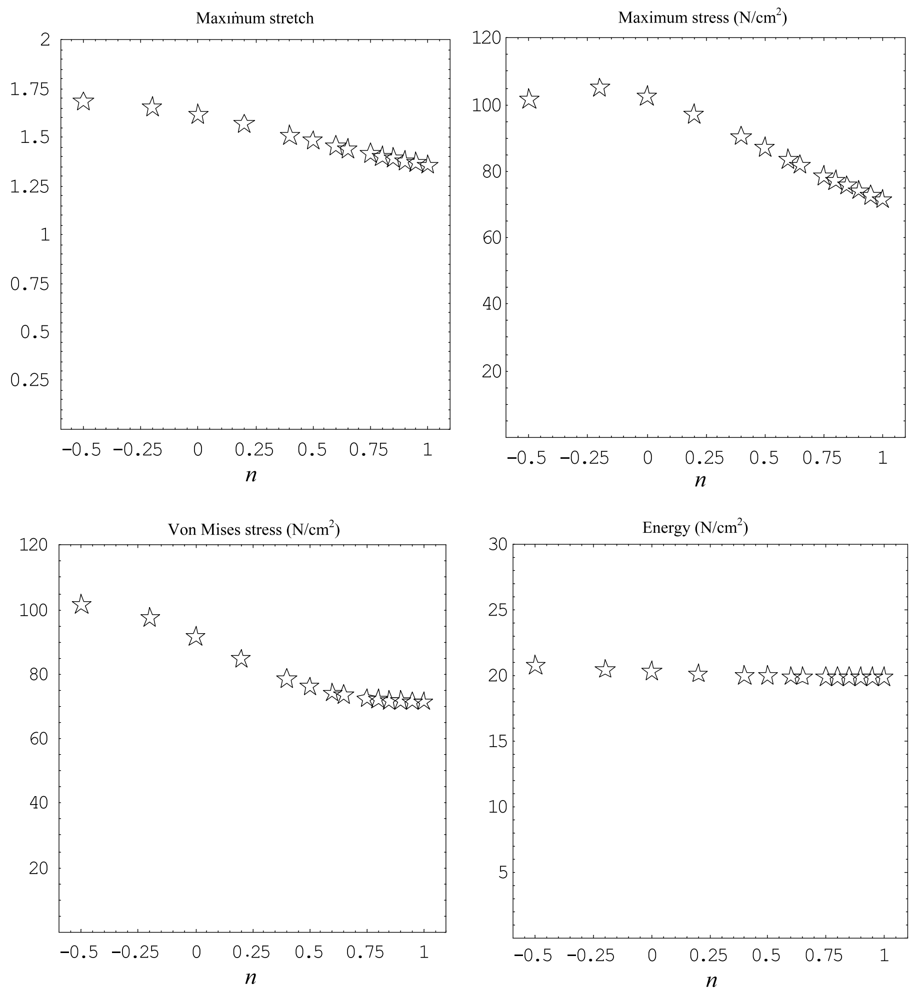

Fig. 5 – Critical failure criteria for Abdominal Aortic Aneurysm under varying biaxiality ratio.

where indices 1, 2, 3 of the components of the Green strain tensor $\mathbf{E}$ designate the axial, circumferential, and radial directions of the artery accordingly; material constants are: $c = 26.95$ KPa; $c_1 = 0.4180$; $c_2 = 0.9925$; $c_3 = 0.0089$; $c_4 = 0.0193$; $c_5 = 0.0749$; $c_6 = 0.0295$; $m = 10$. The Green strain tensor $\mathbf{E} = (\mathbf{F}^T\mathbf{F} - \mathbf{1})/2$ is calculated by using the second-order identity tensor $\mathbf{1}$ and the deformation gradient tensor $\mathbf{F} = \partial\mathbf{y}/\partial\mathbf{x}$ where $\mathbf{x}$ and $\mathbf{y}(\mathbf{x})$ are the referential and current positions of a material point accordingly.

We notice that the model does not include the dependence on shear strains following the original suggestion by Fung because the three axial directions are considered to be principal. Following this setting we can express the homogeneous deformation law and nonzero strains as follows

$$y_1 = \lambda_1 x_1, \qquad y_2 = \lambda_2 x_2, \qquad y_3 = \lambda_3 x_3, \tag{3.4}$$

$$E_{11} = \frac{1}{2}(\lambda_1^2 - 1), \qquad E_{22} = \frac{1}{2}(\lambda_2^2 - 1), \qquad E_{33} = \frac{1}{2}(\lambda_3^2 - 1). \tag{3.5}$$

Based on these kinematic assumptions and the incompressibility condition we have the following constitutive equations

$$\begin{aligned} &\sigma_{11} = -p + \lambda_1^2 \frac{\partial\psi}{\partial E_{11}}, \qquad \sigma_{22} = -p + \lambda_2^2 \frac{\partial\psi}{\partial E_{22}}, \\ &\sigma_{33} = -p + \lambda_3^2 \frac{\partial\psi}{\partial E_{33}}, \end{aligned} \tag{3.6}$$

or

$$\begin{aligned} &\sigma_1 = -p + \lambda_1 \frac{\partial\psi}{\partial\lambda_1}, \qquad \sigma_2 = -p + \lambda_2 \frac{\partial\psi}{\partial\lambda_2}, \\ &\sigma_3 = -p + \lambda_3 \frac{\partial\psi}{\partial\lambda_3}, \end{aligned} \tag{3.7}$$

where p is indefinite Lagrange multiplier.

The incompressibility condition $J = \lambda_1\lambda_2\lambda_3 = 1$ means that one stretch is not independent and, consequently, it is possible to modify the strain energy function as follows

$$\hat{\psi}(\lambda_1, \lambda_2) = \psi(\lambda_1, \lambda_2, \lambda_1^{-1}\lambda_2^{-1}). \tag{3.8}$$

Excluding the Lagrange multiplier from (3.7) and accounting for (3.8) we get

$$\sigma_1 - \sigma_3 = \lambda_1 \frac{\partial\hat{\psi}}{\partial\lambda_1}, \qquad \sigma_2 - \sigma_3 = \lambda_2 \frac{\partial\hat{\psi}}{\partial\lambda_2}, \tag{3.9}$$

or for a thin sheet of material we assume $\sigma_3 = 0$ and obtain

$$\sigma_1 = \lambda_1 \frac{\partial\hat{\psi}}{\partial\lambda_1}, \qquad \sigma_2 = \lambda_2 \frac{\partial\hat{\psi}}{\partial\lambda_2}. \tag{3.10}$$

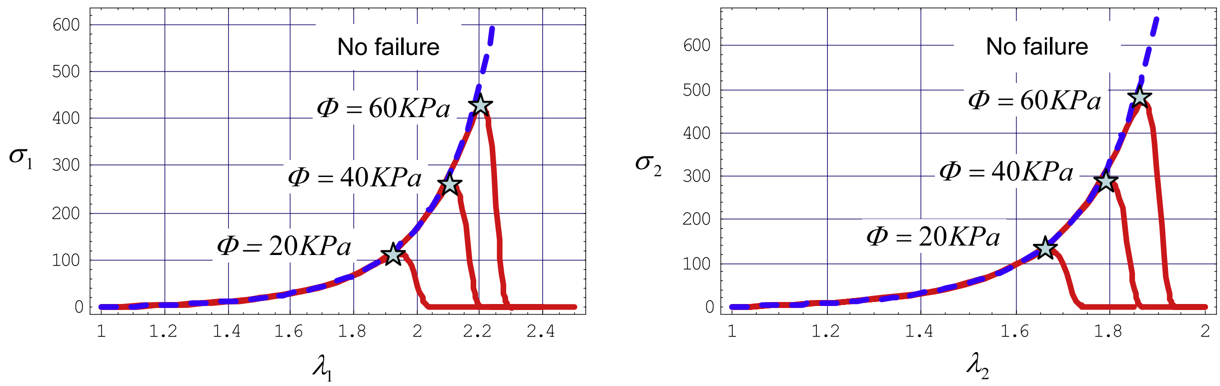

Fig. 6 – Pure shear for the enhanced Fung model: stress [KPa] versus stretch in axial and circumferential directions of the artery.

The stress–stretch curves in pure shear (PS) in axial ($\lambda_1 = \lambda, \lambda_2 = 1$) and circumferential ($\lambda_2 = \lambda, \lambda_1 = 1$) directions are presented in Fig. 6 for varying Φ.

The different graphs presented in Fig. 6 point towards the difference between the isotropic and anisotropic models. The graph on the left and the right of the figure present the pure shear in the axial and circumferential directions of the artery correspondingly. Because of anisotropy the graphs show the different stiffness and strength. Indeed, the increase of the stress–stretch curve in the axial arterial direction is more gradual than in the circumferential direction. Accordingly, the strength, which is the maximum principal stress, in the circumferential direction is higher than in the axial one while the corresponding maximum stretch is lower. Thus, the circumferential direction is stiffer overall than the axial direction.

Fig. 6 also reveals the role of parameter Φ whose increase leads to the increase of strength. It is remarkable that the departure from the stress–stretch curve of the intact material occurs at the point of rupture. The latter is due to the relatively high value of $m = 10$.

We further consider the biaxial tension of an arterial sheet described by the enhanced Fung model (3.1)–(3.3). In this case, which preserves symmetry, formula (3.10) is applicable and we can analyze rupture analogously to the previous section.

We do not know the true value of Φ because of the lack of the experimental data and we arbitrarily choose $\Phi = 40$ KPa for the subsequent calculations.

Fig. 7a presents the local failure criteria at the point of rupture when the sheet is stretched by λ in the axial and by λ^n in the circumferential arterial direction accordingly. Qualitatively, the results are similar to those for isotropic materials considered in the previous section—the local magnitude of the critical energy stays as the most robust failure criteria. There is an interesting point, however, in the obtained results which appears due to anisotropy: the graphs of the maximum principal stress and von Mises stress have a global minimum point. This point indicates the transition from the maximum principal stress in the axial direction, $\sigma_{1\max}$, to the maximum principal stress in the circumferential direction, $\sigma_{2\max}$. This transition occurs because the material is stiffer in the circumferential direction.

Fig. 7b presents the local failure criteria at the point of rupture when the sheet is stretched by λ in the circumferential and by λ^n in the axial arterial direction accordingly. Qualitatively, the results are similar to those for isotropic materials considered in the previous section—the local magnitude of the critical energy stays as the most robust failure criteria. Contrary to the results presented in Fig. 7a there is no point of the transition between the maximum principal stretches in directions 1 and 2. The latter happens because the circumferential direction is stiffer from the point of view of the material and it dominates deformation.

4. First enhanced HGO model

We turn now to another model of the arterial wall (Holzapfel et al., 2000), which became very popular recently. The Holzapfel–Gasser–Ogden (HGO) material model is also incompressible and anisotropic. Contrary to Fung's model, however, anisotropy is introduced with the help of the so-called structural tensors that are formed by the tensor product of the unit vectors in the characteristic directions of anisotropy. The latter idea should probably be credited to Spencer (1972, 1984). We also mention the work by Lanir (1983), which was in effect a predecessor of the rising trend of the so-called multiscale models in soft tissue mechanics.

The HGO model enhanced with the failure description can be written as follows

$$\psi = \frac{\Phi}{m}\left\{\Gamma\left(\frac{1}{m}, 0\right) - \Gamma\left(\frac{1}{m}, \frac{W^m}{\Phi^m}\right)\right\}, \quad (4.1)$$

$$W = \frac{c}{2}(I_1 - 3) + \frac{k_1}{2k_2}\{\exp(k_2(J_1 - 1)^2) + \exp(k_2(J_2 - 1)^2) - 2\}, \quad (4.2)$$

$$I_1 = \mathbf{F} : \mathbf{F}, \qquad J_1 = (\mathbf{F}^T\mathbf{F}) : (\mathbf{M}_1 \otimes \mathbf{M}_1), \qquad J_2 = (\mathbf{F}^T\mathbf{F}) : (\mathbf{M}_2 \otimes \mathbf{M}_2), \quad (4.3)$$

$$\mathbf{M}_1 = (\sin\beta, \cos\beta, 0)^T, \quad \mathbf{M}_2 = (-\sin\beta, \cos\beta, 0)^T, \quad (4.4)$$

where[4] $c = 3.0$ KPa, $k_1 = 2.36$ KPa, $k_2 = 0.84$, $\beta = \pi/6$, $m = 10$; the structural tensors $\mathbf{M}_1 \otimes \mathbf{M}_1$ and $\mathbf{M}_2 \otimes \mathbf{M}_2$ are formed from the unit vectors $\mathbf{M}_1, \mathbf{M}_2$ pointing out the characteristic direction of the collagen fibers which are inclined with angle β with respect to the circumferential direction, 2.

[4] We use the Holzapfel et al. (2000) data for the media layer, which dominates mechanical behavior of the artery.

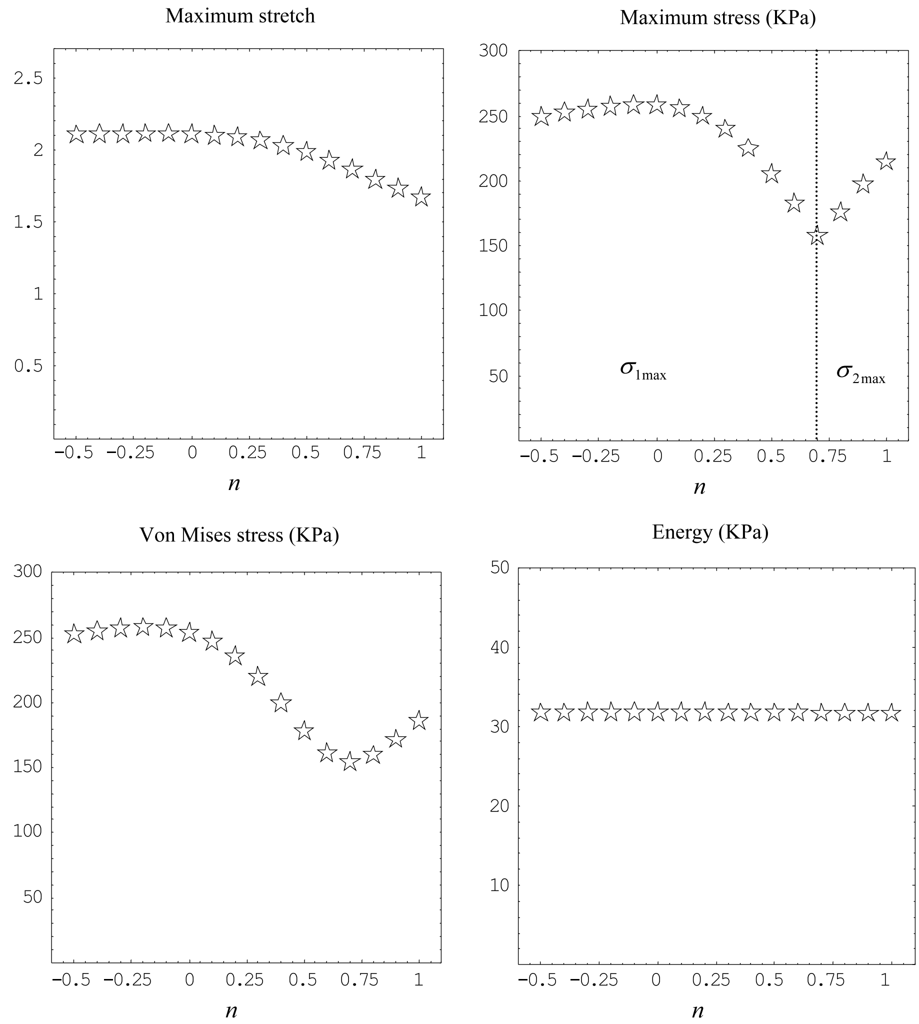

Fig. 7a – Local failure criteria for the enhanced Fung model in biaxial tension: $\lambda_1 = \lambda, \lambda_2 = \lambda^n$.

In the case of the homogeneous deformation described by (3.4) we can express the invariants in (4.3) through the principal stretches that, because of symmetry, coincide with the main arterial directions: axial, circumferential, radial. Thus, we have

$$I_1 = \lambda_1^2 + \lambda_2^2 + \lambda_1^{-2}\lambda_2^{-2}, \qquad J_1 = J_2 = \lambda_1^2 \sin^2\beta + \lambda_2^2 \cos^2\beta, \quad (4.5)$$

where we used the incompressibility condition in the form: $\lambda_3^2 = \lambda_1^{-2}\lambda_2^{-2}$.

Substituting (4.5) in (4.1) and (4.2) we get

$$\hat{\psi}(\lambda_1, \lambda_2) = \psi(I_1, J_1, J_2). \quad (4.6)$$

We can further use Eq. (3.10) for the study of biaxial tension of the enhanced HGO model. Particularly, Fig. 8 presents the stress–stretch curves in pure shear (PS) in axial ($\lambda_1 = \lambda, \lambda_2 = 1$) and circumferential ($\lambda_2 = \lambda, \lambda_1 = 1$) directions are presented for varying Φ.

The graphs in Fig. 8 are qualitatively similar to those in Fig. 6 for Fung's material. There is a quantitative difference, however. Again we observe that the stiffness and the strength are higher in the circumferential direction than in the axial one and the increase of Φ leads to the increase of the strength.

We further investigate the states of biaxial failure under the varying biaxiality parameter $n = \ln\lambda_2/\ln\lambda_1$. Figs. 9a and 9b presents the critical local criteria of the material failure analogously to Figs. 7a and 7b. It is readily observed that the results are qualitatively similar to those for the enhanced Fung material while there is some quantitative difference as expected. Again we observe that anisotropy makes profound effect on the failure criteria. And again the local energy criterion seems to be the most robust.

5. Second enhanced HGO model

Two previous models, considered in Sections 3 and 4, included only one parameter Φ enforcing a failure description. In the absence of the experimental data it is difficult to decide whether this parameter is enough for the failure description. In the present section, we show how to make the models more flexible in fitting the experimental data. The basic idea is to consider anisotropic material as a mixture of constituents enjoying their separate failure descriptions. In effect, this idea has been implemented in Volokh (2008b).

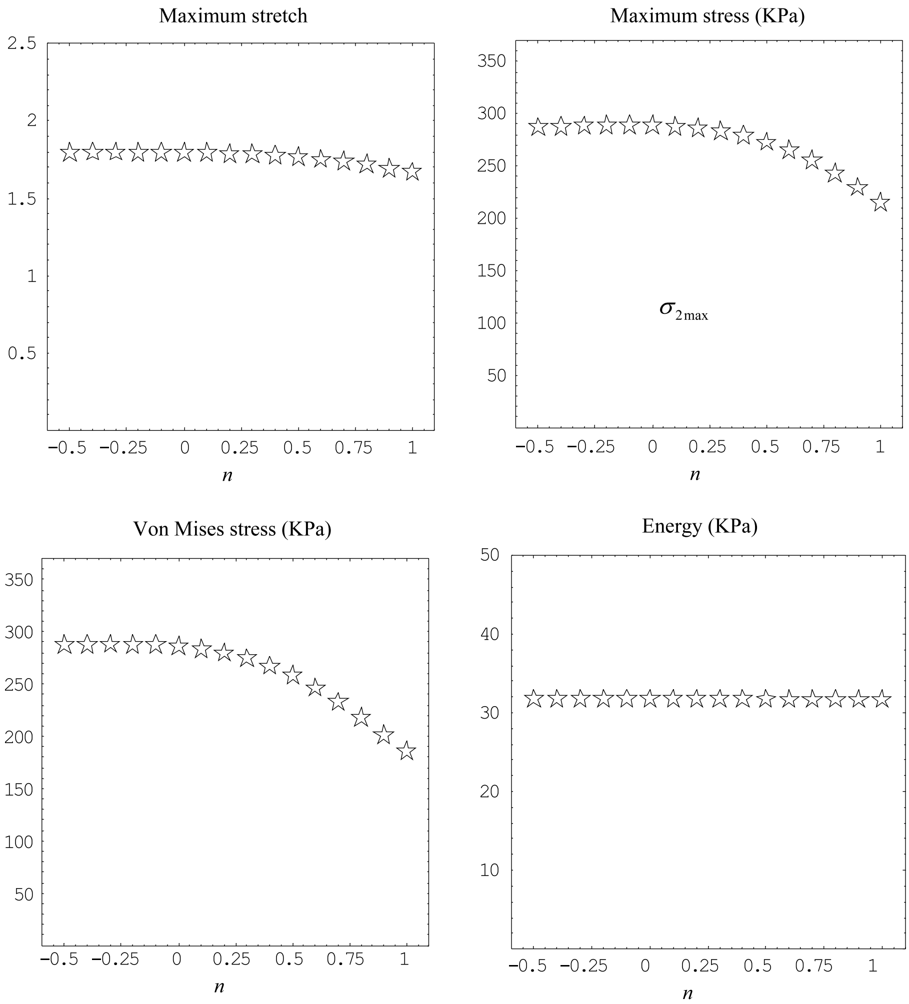

Fig. 7b – Local failure criteria for the enhanced Fung model in biaxial tension: $\lambda_2 = \lambda, \lambda_1 = \lambda^n$.

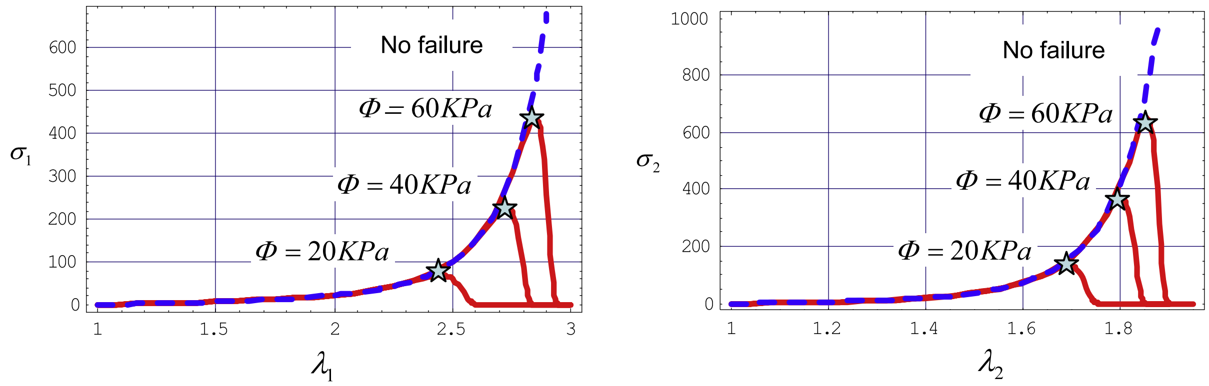

Fig. 8 – Pure shear for the first enhanced HGO model: stress [KPa] versus stretch in axial and circumferential directions of the artery.

However, a description of failure was a bit too complex and not systematic. In the present section we improve on Volokh (2008b) by making the model more general and simple simultaneously. Particularly, we introduce the following strain energy function

$$\psi = \psi_1 + \psi_2 + \psi_3, \tag{5.1}$$

$$\psi_1 = \frac{\Phi_1}{m_1}\left\{\Gamma\left(\frac{1}{m_1}, 0\right) - \Gamma\left(\frac{1}{m_1}, \frac{W_1^{m_1}}{\Phi_1^{m_1}}\right)\right\}, \tag{5.2}$$

$$W_1 = \frac{c}{2}(I_1 - 3), \tag{5.3}$$

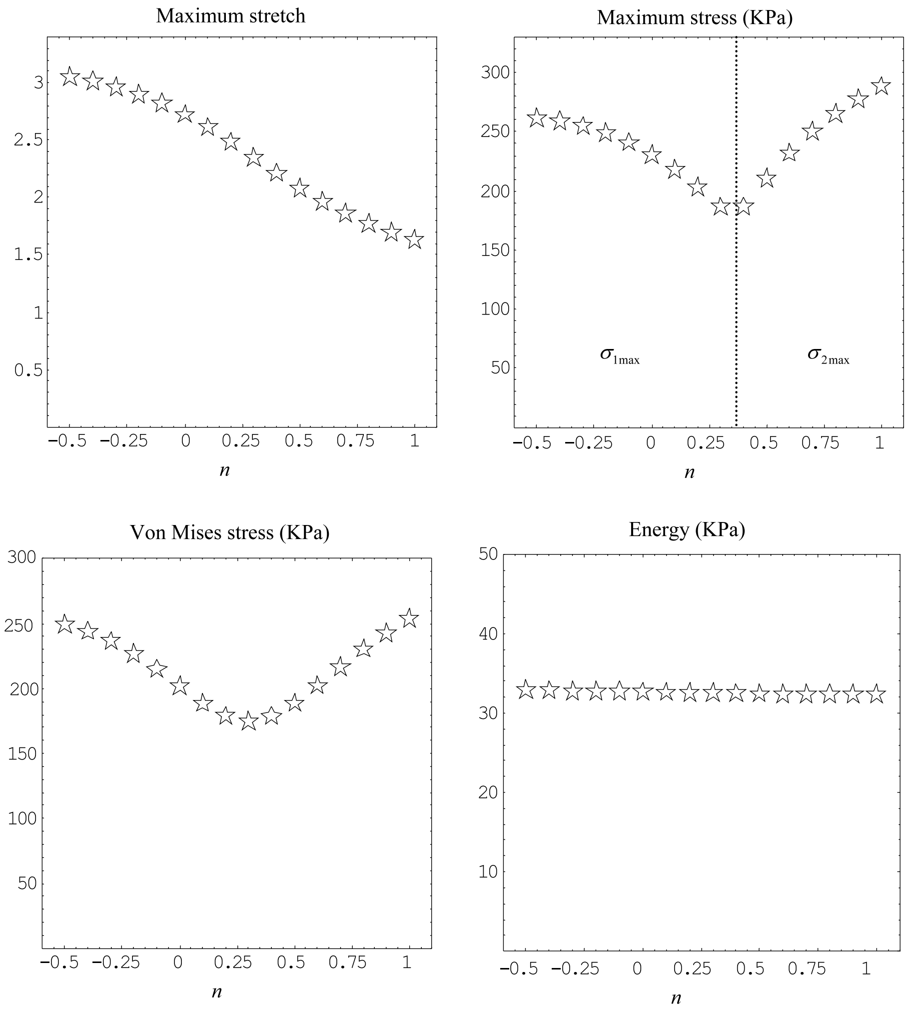

Fig. 9a – Local failure criteria for the first enhanced HGO model in biaxial tension: $\lambda_1 = \lambda, \lambda_2 = \lambda^n$.

$$\psi_2 = \frac{\Phi_2}{m_2}\left\{\Gamma\left(\frac{1}{m_2}, 0\right) - \Gamma\left(\frac{1}{m_2}, \frac{W_2^{m_2}}{\Phi_2^{m_2}}\right)\right\}, \tag{5.4}$$

$$W_2 = \frac{k_1}{2k_2}\{\exp(k_2(J_1 - 1)^2) - 1\}, \tag{5.5}$$

$$\psi_3 = \frac{\Phi_3}{m_3}\left\{\Gamma\left(\frac{1}{m_3}, 0\right) - \Gamma\left(\frac{1}{m_3}, \frac{W_3^{m_3}}{\Phi_3^{m_3}}\right)\right\}, \tag{5.6}$$

$$W_3 = \frac{k_1}{2k_2}\{\exp(k_2(J_2 - 1)^2) - 1\}. \tag{5.7}$$

Here ψ_1 describes the mechanical response of the isotropic matrix while ψ_2 and ψ_3 describe the response of two families of fibers accordingly. Every constituent has its own failure parameters Φ_i and m_i that can be fitted independently.

To be specific we assume: $m_i = 10, c = 3.0$ KPa, $k_1 = 2.36$ KPa, $k_2 = 0.84, \beta = \pi/6$, like in the previous section. Besides, we fix $\Phi_1 = 10$ KPa in all subsequent computations and we only vary $\Phi_2 = \Phi_3 = 10; 15; 20$ KPa.

Again, we use Eq. (3.10) for the study of biaxial tension of the second enhanced HGO model. Fig. 10 presents the stress–stretch curves in pure shear (PS) in axial ($\lambda_1 = \lambda, \lambda_2 = 1$) and circumferential ($\lambda_2 = \lambda, \lambda_1 = 1$) directions are presented for varying $\Phi_2 = \Phi_3$.

Similar to the already considered models we observe that the stiffness and the strength are higher in the circumferential direction than in the axial one and the increase of $\Phi_2 = \Phi_3$ leads to the increase of the strength.

The critical failure criteria are analyzed in Fig. 11.

As compared to the previous models we notice a slight scattering for the data on the critical failure energy around the magnitude of 30 KPa.

6. Discussion

In the present work we developed new models of soft anisotropic materials considering a description of the mechanical behavior of the arterial wall. The main feature of the developed models is the account of material failure in constitutive equations. The latter is achieved by setting the limits for the accumulation of the strain energy. These limits lead to the appearance of the limit point on the stress–strain curve indicating material instability and failure. An attractive aspect of the proposed approach is the possibility to enhance the already existing and successful models of intact materials with a failure description. We

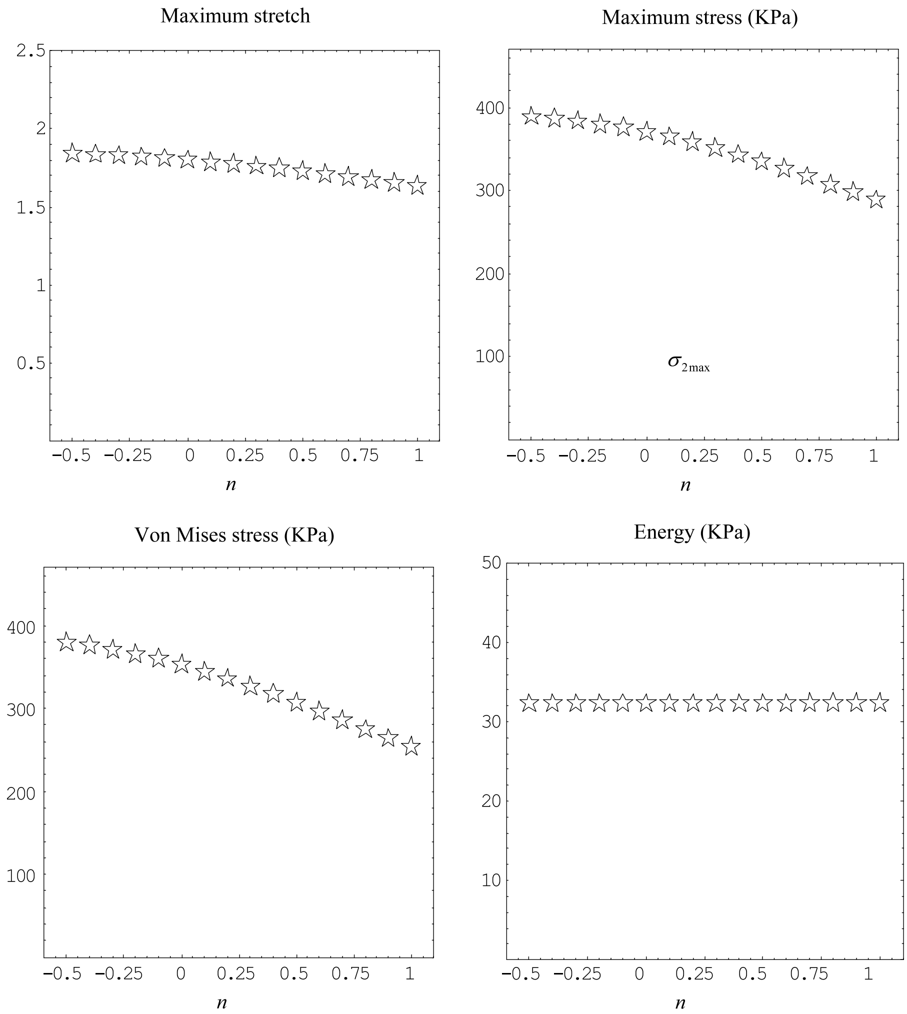

Fig. 9b – Local failure criteria for the first enhanced HGO model in biaxial tension: $\lambda_2 = \lambda$, $\lambda_1 = \lambda^n$.

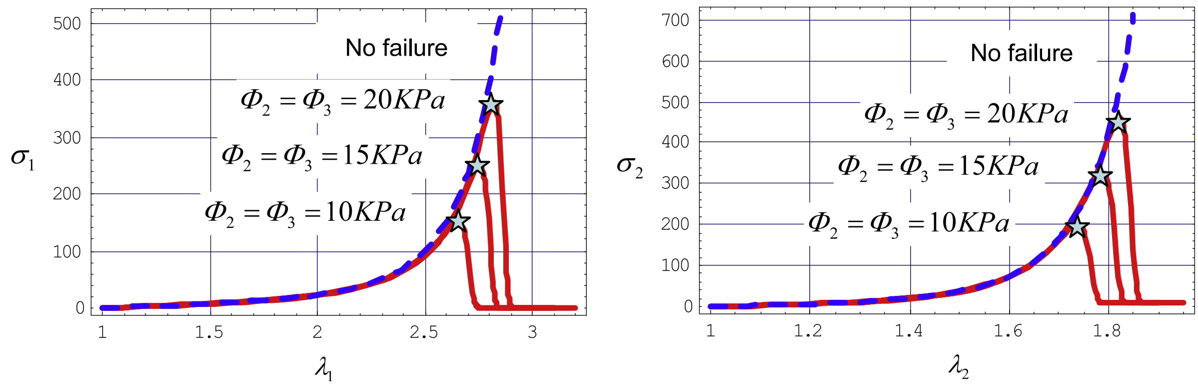

Fig. 10 – Pure shear for the second enhanced HGO model: stress [KPa] versus stretch in axial and circumferential directions of the artery.

emphasize, however, that the proposed approach is not universal: materials exhibiting essential structural changes during deformation, e.g. plasticity, are beyond the scope of the methods of energy limiters.

Particularly, we enhanced the Fung and the Holzapfel–Gasser–Ogden models of anisotropic soft tissue with the energy limiters. The new enhanced models were used for analysis of rupture of a material sheet under tension with the varying biaxiality ratio. The found rupture conditions were used for the calculation of some basic failure criteria including the maximum principal stretch and stress, the von Mises stress, and the strain energy. The calculation showed

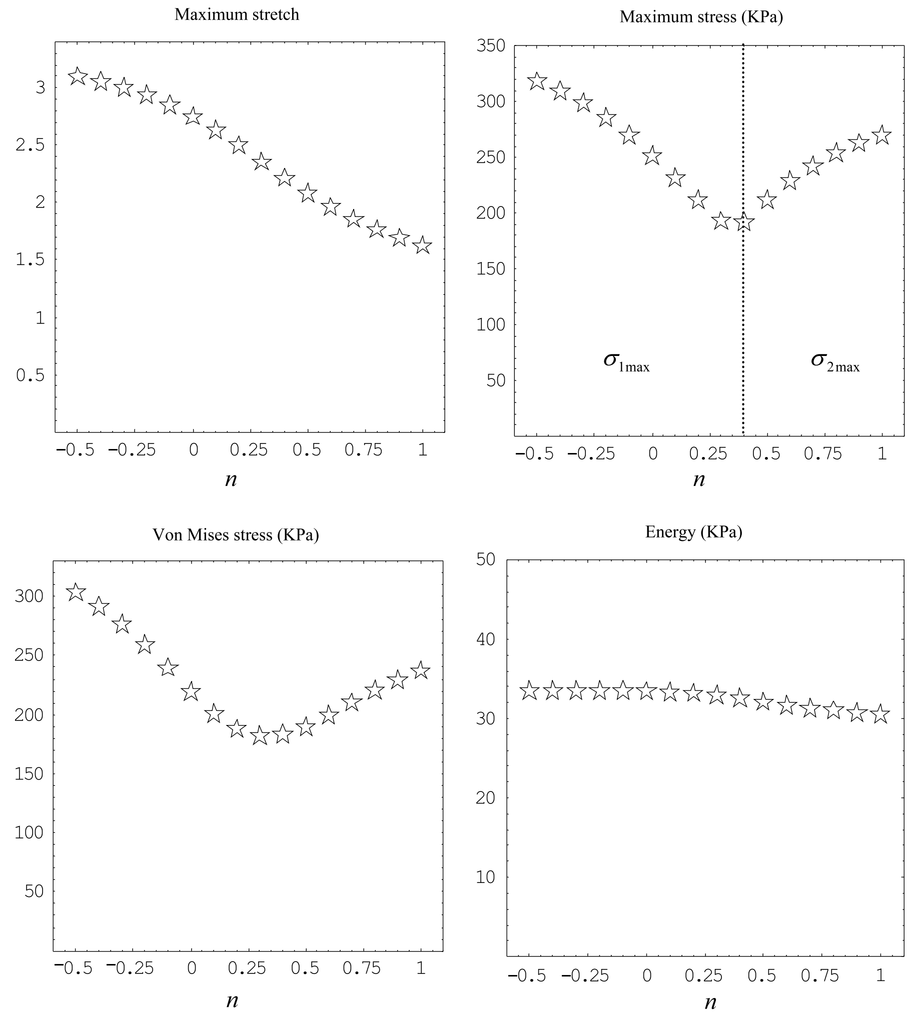

Fig. 11a – Local failure criteria for the second enhanced HGO model in biaxial tension: $\lambda_1 = \lambda, \lambda_2 = \lambda^n$.

that only the strain energy magnitude corresponding to the point of rupture exhibited a small scattering while other criteria altered significantly under the variation of the stress state from the uniaxial tension to the equal biaxial tension. Moreover, the effect of anisotropy on these alterations was pronounced.

It is remarkable that the maximum principal stretches and stresses as well as the critical von Mises stress derived in the uniaxial tension tests cannot be used as the failure criteria for the stress–strain states with the developed biaxiality because in the latter case the critical stretches and stresses have soundly lower magnitudes than in the case of the uniaxial tension.[5] The comprehension and appreciation of this fact is crucial and it is, probably, the main practical lesson to be learned from the present theoretical study.

One might argue that the considered failure criteria are not the criteria of the choice in the case of the fiber-reinforced composites. Indeed, Bower (2010) suggests the following criteria for anisotropic materials, for example.

The criterion of the *orientation dependent fracture strength* is described by the following inequality for an orthotropic material

$$\max_{\theta,\varphi} \frac{n_i(\theta,\varphi)\sigma_{ij}n_j(\theta,\varphi)}{(\sigma_{TS1}\cos^2\theta + \sigma_{TS2}\sin^2\theta)\sin^2\varphi + \sigma_{TS3}\cos^2\varphi} \le 1, \qquad (6.1)$$

where unit vector $\mathbf{n}(\theta,\varphi)$ is defined by its spherical angular coordinates θ and φ with respect to the orthotropy directions and $\sigma_{TS1}, \sigma_{TS2}, \sigma_{TS3}$ are the tensile strength magnitudes in the directions of orthotropy.

It is vital to note that though the tensile strengths are used for all orthotropy directions their values are defined in *uniaxial tension tests*. The results of the present work, however, show that the uniaxial tension tests do not provide enough information for establishing the local stress-based failure criteria in the case of the multiaxial stress state.

Another possible critical condition for a fiber-reinforced composite is the *Tsai-Hill criterion* that can be written as follows for the plane stress state

$$\frac{\sigma_{11}^2}{\sigma_{TS1}^2} + \frac{\sigma_{22}^2}{\sigma_{TS2}^2} - \frac{\sigma_{11}\sigma_{22}}{\sigma_{TS1}^2} + \frac{\sigma_{12}^2}{\sigma_{SS}^2} \le 1, \qquad (6.2)$$

where index 1 designates the direction of fibers and index 2 designates the orthogonal direction.

[5] See also Appendix.

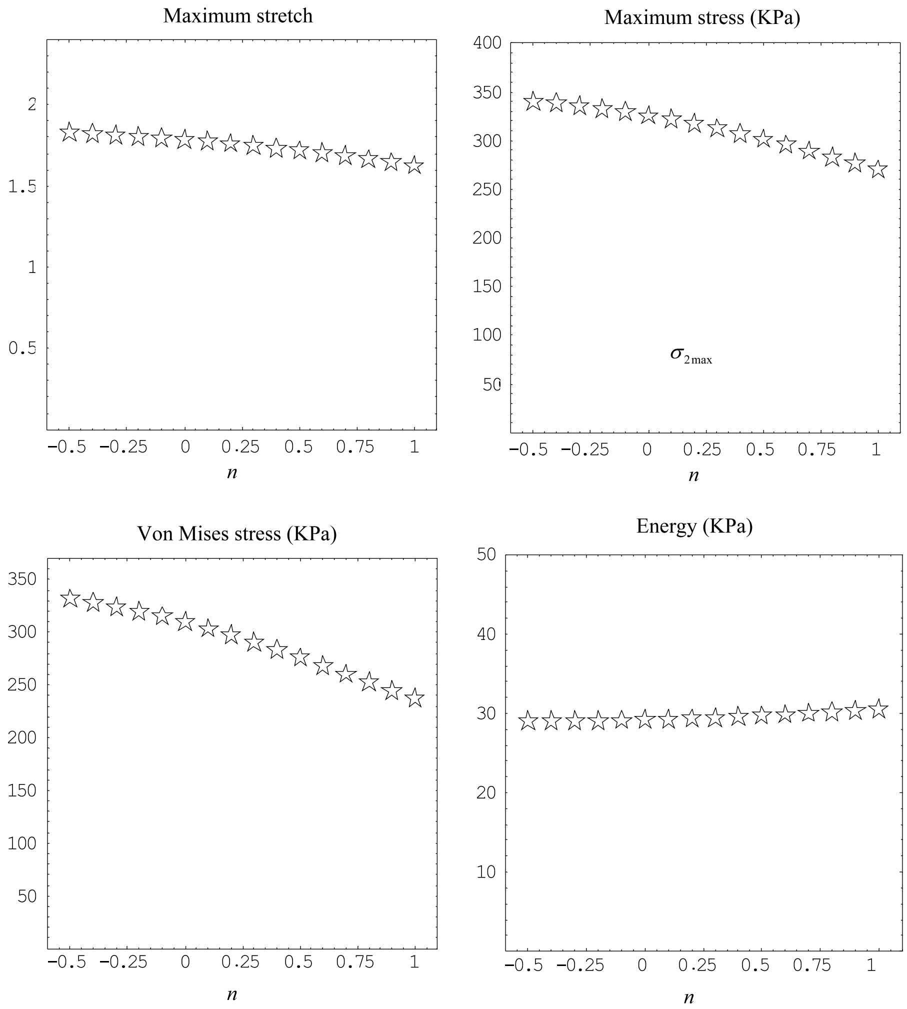

Fig. 11b – Local failure criteria for the second enhanced HGO model in biaxial tension: $\lambda_2 = \lambda, \lambda_1 = \lambda^n$.

Tensile strengths $\sigma_{TS1}, \sigma_{TS2}$ are derived in uniaxial tension tests while shear strength σ_{SS} can be expressed through $\sigma_{TS1}, \sigma_{TS2}$ (see Bower (2010) for details). Again the uniaxial tension experiments are assumed to be enough for establishing the multiaxial fracture criteria contrary to the results of the present work.

It is our hope and purpose that the results of the present study will encourage the experimentalists to do failure tests in the biaxial tension. Such tests are a great challenge because the biaxial tension and failure are very sensitive to imperfections in materials and loads. The only work we know where the biaxial tension including failure was monitored is the study by Hamdi et al. (2006) whose results we used in Section 2. In that work the rubber balloon was inflated up to rupture under the varying radius of the stiff meniscus fixing the balloon. While this sort of experiment is suitable for rubber it is hardly doable for the living tissue.[6] It is probably possible to suggest another experimental design for a tissue sample. The idea is to stretch the tissue sheet in the first direction and then to fix the stretch by using a device which can slide freely in the perpendicular direction. After that it is possible to stretch the sheet up to rupture in the second perpendicular direction. By changing the initial pre-stretch it is possible to obtain the biaxial failure data of the type presented in Figs. 7, 9 and 11. The proposed scheme does not require the *simultaneous* loading in two directions which is difficult to perform and can probably be more attractive practically.

[6] We would be happy to find this statement wrong.

Appendix

The comparisons of various local failure criteria have been made in the paper based on the models of elasticity with energy limiters. It might also be interesting to directly compare the local failure criteria established in the uniaxial tension tests to the experimental data on natural rubber presented in Fig. 3. Such a comparison is shown in Fig. A.1 for the critical von Mises stress and the maximum principal stress calculated based on the intact rubber model described by Eq. (2.4). We also notice that criterion (6.1) coincides with the maximum principal stress for isotropic materials.

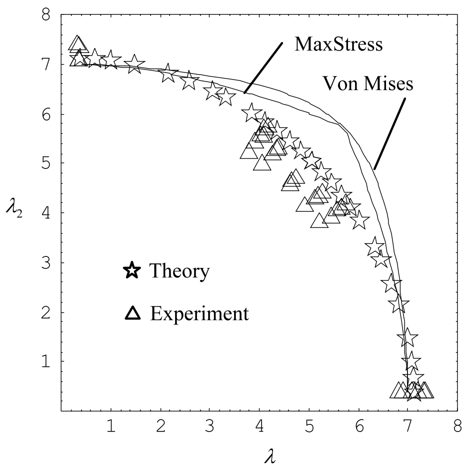

Fig. A.1 – Critical failure stretches in biaxial tension for natural rubber.

REFERENCES

Balzani, D., Schroeder, J., Gross, D., 2006. Simulation of discontinuous damage incorporating residual stresses in circumferentially overstretched atherosclerotic arteries. Acta Biomater. 2, 609–618.

Beatty, M.F., 1987. Topics in finite elasticity: hyperelasticity of rubber, elastomers and biological tissues—with examples. Appl. Mech. Rev. 40, 1699–1734.

Bower, A.F., 2010. Applied Mechanics of Solids. CRC Press.

Calvo, B., Pena, E., Martinez, M.A., Doblare, M., 2006. An uncoupled directional damage model for fibred biological soft tissues. Formulation and computational aspects. Internat. J. Numer. Methods Engrg. 69, 2036–2057.

Chuong, C.J., Fung, Y.C., 1983. Three-dimensional stress distribution in arteries. J. Biomech. Eng. 105, 268–274.

Cowin, S.C., Humphrey, J.D., 2002. Cardiovascular Soft Tissue Mechanics. Springer, New York.

Fung, Y.C., 1993. Biomechanics: Mechanical Properties of Living Tissues, 2nd ed. Springer, New York.

Fung, Y.C., Fronek, K., Patitucci, P., 1979. Pseudoelasticity of arteries and the choice of its mathematical expression. Am. J. Physiol. 237, H620–H631.

Hamdi, A., Nait Abdelaziz, M., Ait Hocine, N., Heuillet, P., Benseddiq, N., 2006. A fracture criterion of rubber-like materials under plane stress conditions. Polym. Test. 25, 994–1005.

Hokanson, J., Yazdami, S., 1997. A constitutive model of the artery with damage. Mech. Res. Comm. 24, 151–159.

Holzapfel, G.A., Gasser, T.C., Ogden, R.W., 2000. A new constitutive framework for arterial wall mechanics and a comparative study of material models. J. Elasticity 61, 1–48.

Holzapfel, G.A., Ogden, R.W., 2003. Biomechanics of Soft Tissues in Cardiovascular Systems. Springer, Wien.

Holzapfel, G.A., Ogden, R.W., 2006. Mechanics of Biological Tissue. Springer, Wien.

Holzapfel, G.A., Ogden, R.W., 2010. Constitutive modeling of arteries. Proc. R. Soc. Lond. Ser. A 466, 1551–1597.

Humphrey, J.D., 2002. Cardiovascular Solid Mechanics: Cells, Tissues, and Organs. Springer, New York.

Lanir, Y., 1983. Constitutive equations for fibrous connective tissues. J. Biomech. 16, 1–12.

Ogden, R.W., 2003. Nonlinear elasticity, anisotropy, material stability and residual stresses in soft tissue. In: Holzapfel, G.A., Ogden., R.W. (Eds.), Biomechanics of Soft Tissue in Cardiovascular Systems. In: CISM Courses and Lectures, vol. 441. Springer, Vienna, Austria, pp. 65–108.

Rodriguez, J.-F., Cacho, F., Bea, J.A., Doblare, M., 2006. A stochastic structurally based three dimensional finite strain damage model for fibrous soft tissue. J. Mech. Phys. Solids 54, 564–886.

Spencer, A.J.M., 1972. Deformation of Fibre-Reinforced Materials. Oxford University Press.

Spencer, A.J.M., 1984. Constitutive theory for strongly anisotropic solids. In: Spencer, A.J.M. (Ed.), Continuum Theory of the Mechanics of Fibre-Reinforced Composites. In: CISM Courses and Lectures, vol. 282. Springer-Verlag, Wien, pp. 1–32.

Trapper, P., Volokh, K.Y., 2010. Modeling dynamic failure in rubber. Int. J. Fract. 162, 245–253.

Vande Geest, J.P., Sacks, M.S., Vorp, D.A., 2006. The effect of aneurysm on the biaxial mechanical behavior of human abdominal aorta. J. Biomech. 39, 1324–1334.

Volokh, K.Y., 2007. Hyperelasticity with softening for modeling materials failure. J. Mech. Phys. Solids 55, 2237–2264.

Volokh, K.Y., 2008a. Multiscale modeling of material failure: From atomic bonds to elasticity with energy limiters. J. Multiscale Comput. Eng. 6, 393–410.

Volokh, K.Y., 2008b. Prediction of arterial failure based on a microstructural bi-layer fiber-matrix model with softening. J. Biomech. 41, 447–453.

Volokh, K.Y., 2010a. On modeling failure of rubberlike materials. Mech. Res. Comm. 37, 684–689.

Volokh, K.Y., 2010b. Comparison of biomechanical failure criteria for abdominal aortic aneurysm. J. Biomech. 43, 2032–2034.

Volokh, K.Y., 2011. Characteristic length of damage localization in rubber. Int. J. Fract. 168, 113–116.

Volokh, K.Y., Vorp, D.A., 2008. A model of growth and rupture of abdominal aortic aneurysm. J. Biomech. 41, 1015–1021.